Volume 54
Number 1
4 January 2018
Pages 1-112

ChemComm

Chemical Communications

rsc.li/chemcomm

ISSN 1359-7345

COMMUNICATION
S. J. Connon, M. O. Senge et al.
Conformational control of nonplanar free base porphyrins: towards bifunctional catalysts of tunable basicity

ROYAL SOCIETY
OF CHEMISTRY

rsc.li/chemcomm

Please do ChemComm margins

Journal Name

COMMUNICATION

Fluorinated porous organic frameworks for improved CO$_2$ and CH$_4$ capture

A. Comotti, F. Castiglioni, S. Bracco,* J. Perego, A. Pedrini, M. Negroni and P. Sozzani

Porous 3D selectively-fluorinated framework (F-PAF1), robust yet flexible and with a surface area of 2050 m^2/g, was synthesised by condensation of *ad hoc* prepared fluorinated tetraphenylmethane (TPM) monomer to ensure homogenously distributed C-F dipoles in the swellable architecture. Tetradentate TPM was also the comonomer for the reaction with fluorinated difunctional monomers to obtain frameworks (FMFs) with a controlled amount of regularly spaced reorientable C-F dipoles. Isosteric heat of adsorption of CO$_2$ was incremented of 53% by even moderate C-F dipoles insertion, with respect to the non-fluorinated frameworks. CO$_2$/N$_2$ selectivity was also increased up to a value of 50 for the difluoro-containing comonomer. Moreover, methane shows optimal interaction energies of 24 kJmol^{-1}.

Carbon dioxide is undisputedly one of the major causes for the global warming phenomenon and it is also involved in other serious environmental issues, such as the incremented acidity of oceans.[1] Industrial activity has a critical fallout on CO$_2$ emissions and the most employed technique to reduce its concentration from flue gas streams utilizes amine solutions to chemically bind carbon dioxide molecules.[2] However, this process requires high regeneration costs and produces a negative impact on the environment. In recent years porous materials have emerged as a viable alternative for carbon dioxide capture.[3-5] The main advantages offered by porous solids are the low regeneration costs and superior cyclability provided by gas-solid physisorption phenomena and simpler end-of-life disposal. The classes of materials proposed for this application include Metal-Organic Frameworks (MOFs),[6] HyperCrosslinked Polymers (HCPs),[7] Covalent-Organic Frameworks (COFs),[8] and Porous Organic Frameworks (POFs).[9,10] Since thermal and chemical robustness as well as the versatility of synthesis are required, porous organic frameworks sustained by rigid covalent bonds were a successful choice,

owing to their tough backbone. These materials can exhibit high surface area, large pore volume and remarkable loading capacity.[11-13] However, unfunctionalized POFs have moderate CO$_2$/N$_2$ selectivity. Increased performances for CO$_2$ over N$_2$ is crucial since flue gas streams typically contain 85% N$_2$ and only 15% CO$_2$. A strategy to improve selectivity consists in inserting electron rich functional groups, by pre- and post-synthetic approaches, that are expected to increase the materials affinity towards CO$_2$.[14–18] A variety of functional groups, such as amines, amides and sulfonates, have been tested for this goal.[19–22] Fluorine is a promising candidate since its small size is expected to slightly reduce the total pore volume, while its high electronegativity should establish stronger interactions with CO$_2$ electrical quadrupole moment. So far, a small number of fluorine-functionalized porous organic materials have been explored as adsorbents of CO$_2$.[15,23–25] To extend the library of existing fluorinated organic porous materials, we report the synthesis of new fluorinated organic porous materials by adopting two distinct strategies: direct condensation of an *ad hoc* fluorinated tetrahedral monomer, specifically designed for this sake, and copolymerization between two complementary functionalities of tetrahedral (A$_4$) and fluorine-containing linear (B$_2$) struts such as monofluoro and difluoro-*p*-phenylene units. By this synthetic strategy the fluorine atoms are regularly bound onto each monomeric unit and are exposed to the pore volume (Figure 1).
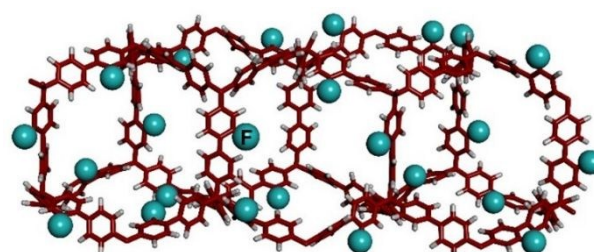
Figure 1 Schematic representation of fluoro porous aromatic framework F-PAF1. Blue spheres represent fluorine atoms.

Our design was to build local C-F dipoles that imparted a dipole moment to the whole *p*-phenylene moiety, wherein C-F groups are inserted. This was made possible by arranging the dipolar

Department of Materials Science, University of Milano Bicocca, via R. Cozzi 55, 20125, Milano, Italy.
E-mail: silvia.bracco@unimib.it

COMMUNICATION

sostituents in a non-centrosymmetric manner. The frameworks were designed to bear a limited amount of fluorine atoms in order to keep the skeleton as light as possible and at the same time a regularly-spaced fluorine substitution. Such homogeneous distribution ensures that the carbon-fluorine dipoles are exposed to the diffusing-in gases, resulting in a well-distinct behaviour as compared to the unfluorinated skeleton and promoting enhanced affinity for CO_2 and CH_4.

The syntheses of the three fluorinated materials are reported in Scheme 1. In particular, the condensation of fluorinated microporous frameworks (FMFs) employs a Sonogashira coupling protocol to create an extended copolymer framework between tetrakis(4-bromophenylmethane) (1) and a difunctional 1,4-diethynil-2-fluorobenzene (2) or 1,4-diethynil-2,3-difluorobenzene (3) in a 1:2 ratio, leading to the formation of 1-FMF and 2-FMF, respectively. The fluorinated porous aromatic framework F-PAF1 was prepared by Yamamoto-type homopolymerization reaction of 4,4',4''-((4-bromo-3-fluorophenyl) methantryl)tris(bromobenzene) (4). To the best of our knowledge, this is the first example of the fluorinated PAF1 carrying the fluorine atoms on the tetraphenylmethane monomer unit.
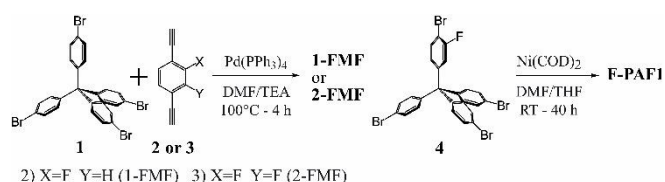
Scheme 1 Schematic synthesis of 1-FMF, 2-FMF and F-PAF1.

The high conversion efficiency of the Cu-free Sonogashira protocol and the formation of alkyne-aryl bonds for the preparation of 1-FMF and 2-FMF was confirmed by FTIR spectroscopy measurements (see ESI, Figure S1). In both IR spectra, the bands ascribable to internal (*i.e.* disubstituted) alkyne groups con be appreciated at 2200 cm^{-1}. TGA curves of the fluoro-containing frameworks show their extremely high stability, up to 450-500°C, as a consequence of the fully covalent bond network (ESI, Figure S2). No periodic order was observed in the powder X-ray diffraction patterns. SEM images of F-PAF1 highlights the narrow distribution of spherical nanoparticles with an average diameter of 78 nm (Figure S4).

Magic angle spinning (MAS) ^{13}C CP NMR spectra show the chemical structure of the frameworks (Figure 2). Signal assignments were established by comparison to solution ^{13}C-NMR spectra of the monomers. Besides the signals of non fluorinated moieties, characteristic signals of the presence of fluorine atoms on *p*-phenylene rings appear in the aromatic region (highlighted orange). The peak at 65 ppm belongs to the central quaternary carbon atom of the tetraphenylmethane units, while the resonances in the 80-100 ppm region of 1-FMF and 2-FMF correspond to C≡C carbon atoms. Notably, in F-PAF1 the doublet due to the 250 Hz J(^{13}C-^{19}F) coupling of the carbon nucleus directly bonded to fluorine atom is apparent at ca. 160 ppm (Figure 2a). ^{13}C T_1 NMR relaxation times indicate fast 10^8 Hz reorientation rate for the non-fluorinated *para*-phenylenes

(T_1=1.5 s for C_3), as occurring in prototypal PAF-1 rotors.[26,27] Despite a comparable torsional flexibility of fluorinated rings about the pivotal sp^2-sp^2 carbon-carbon bonds, orientational dynamics of fluorinated rings was slower, as proved by longer spin-lattice relaxation times (T_1>10s) owing to the increased inertial mass of the rotor and long-range electrostatic interactions among C-F dipoles. Overall, dynamical results depict a skeleton bearing reorientable aromatic moieties, potentially adaptable after guest diffusion. In the 2-FMF spectrum, the C-F signal resonates upfield at 153 ppm (Figure 2c), falling to the side of the dominant resonances of hydrocarburic aromatic carbons, as supported by ^{13}C solution NMR spectrum of the monomer 3 (see ESI). 600 MHz ^{1}H MAS NMR spectra with high spinning speed (35 kHz), which reduced homonuclear dipolar couplings, display exclusively the aromatic signals at δ=6.8 ppm, ensuring the absence of any unreacted monomer or solvent entrapped in the framework as expected for an empty porous structure.
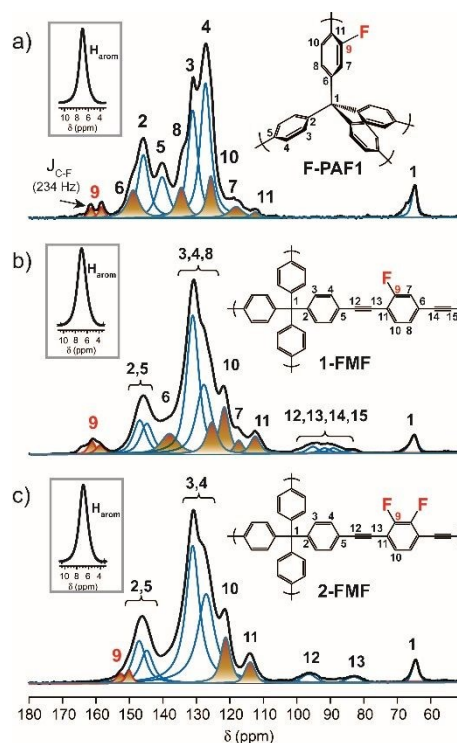

Figure 2 ^{13}C CP MAS NMR spectra of a) F-PAF1, b) 1-FMF and c) 2-FMF (contact time= 2 ms). 600 MHz ^{1}H MAS NMR spectra at 35 kHz spinning speed are reported on the upper left corners. The signals of the fluorinated *p*-phenylene units are highlighted in orange.

The porosity of the materials was evaluated by N_2 adsorption/desorption isotherms at 77 K (Figure 3). The main parameters derived from gas adsorption measurements are reported in Table S1. The Langmuir and BET surface areas of F-PAF1 are 2338 and 2054 m^2/g, respectively: these values are among the highest reported for fluorinated organic porous materials.[15,23-25] The shape shows a contribution by the mesoporosity resulting in a total pore volume of 1.96 cm^3 g^{-1}, that is outstanding for a fluorinated organic porous material. N_2 desorption branch runs distinctly above the adsorption curve, forming a large hysteresis loop closing only at very low

ChemComm

pressures, indicative of framework flexibility owing to the ability of the porous structure of breathing and swelling by absorption, like a sponge.[28] Pore size distribution analysis (PSD), carried out by Non-Local Density Functional Theory (NLDFT) and carbon slit pore model, shows a peak centered at 11.9 Å.
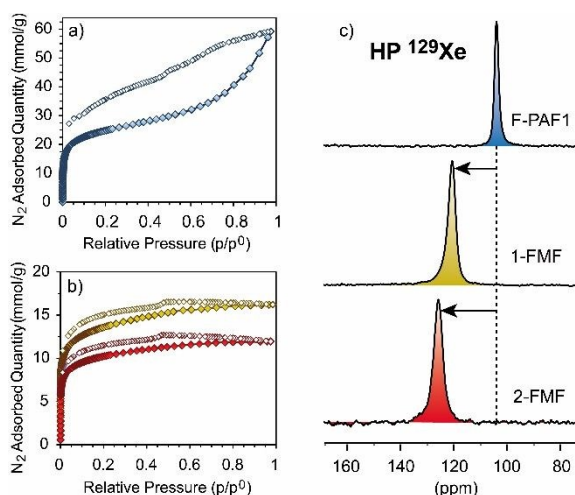

Figure 3 N_2 isotherms at 77 K of F-PAF1 (a) and 1-FMF and 2-FMF (b) (yellow and red diamonds, respectively). c) Hyperpolarized (HP) ^{129}Xe NMR spectra collected at room temperature.

1-FMF and 2-FMF show type I isotherms characteristic of microporous solids with Langmuir and BET surface areas of 1285 and 1132 m^2g^{-1} for 1-FMF and 970 and 853 m^2g^{-1} for 2-FMF, respectively (Figure 3b). PSD analysis reveals two peaks at ca. 5.9 -11.9 Å for 1-FMF and 2-FMF. An increase in the 5.9 Å peak height is observed for the difluoro substituted material (ESI), indicating that the increase of fluorine substitution selects an ultramicroporosity range, which offers neat advantages for the adsorption of small gas molecules. Hyperpolarized (HP) ^{129}Xe NMR is a valuable tool to provide a highly sensitive response to the pore size.[29,30] The exploration of the restricted environment by Xe atoms is manifested by high chemical shift values (104-127 ppm) with respect to the gas phase (Figure 3c). The chemical shift increase from F-PAF1 to copolymers reveals the more effective Xe confinement in the smaller pores of the copolymers (from 11 to 6 Å).

The new fluorinated matrices were tested for carbon dioxide and methane capture. CO_2 sorption isotherms were collected at 195 K up to 1 bar and at three other distinct temperatures (273, 283, 298 K) up to 10 bar (Figure 4a and S8). Owing to its higher surface area, F-PAF1 shows a remarkable CO_2 uptake at 195 K and 1 bar, reaching the value of 26.3 mmol/g, that corresponds to 115% of its weight. Interestingly, in F-PAF1, the CO_2 adsorption value at 273 K and 1 bar is superior to that reported for the unfunctionalized PAF1 (2.7 vs 2.0 mmol/g, respectively),[31] despite the lower BET surface area (2054 vs 5300 m^2/g, respectively). The presence of fluorine atoms enhances low-pressure CO_2 capture through favorable electrostatic interactions. Similarly, the CO_2 uptake for 1-FMF at 273 K and 1 bar is superior to its non-fluorinated analogue MOP1 (2.4 versus 2.1 mmol/g, respectively).[14] Furthermore, the CO_2 isosteric heat of adsorption Q_{st}, calculated using the

vant'Hoff equation at low coverage for F-PAF1 is 25 kJ/mol, which is significantly higher than the 15.6 kJ/mol determined for PAF1.[21] Notably, the CO_2 isotherm changes from a sigmoidal shape for PAF1 to a Langmuir profile for F-PAF1, owing to a higher CO_2 affinity towards the fluorinated surface. Thus, the use of a fluorinated building block leads to a 53% increase of $Q_{st}(CO_2)$ with respect to the non-fluorinated analogue. For 1-FMF, the $Q_{st}(CO_2)$ calculated at low coverage is 30 kJ/mol, respectively, indicating favorable interactions with CO_2. These values are higher than that of the parent non-fluorinated framework (26 kJ/mol), demonstrating the effectiveness of the C-F dipole insertion to enhance the CO_2 capture. It is expected that two vicinal fluorine atoms further increase the binding energy because of the cooperative interactions with the positively charged carbon of CO_2, as previously proved by theoretical calculations.[32] Indeed, for 2-FMF the Q_{st} reached 32 kJ/mol. Futhermore, the torsional flexibility of the Csp_2-Csp bond about the monofluoro and difluoro-p-phenylene moieities[33] may allow to adjust the conformation in order to maximize the dipole-CO_2 interaction.

The higher CO_2 heat of adsorption for the fluorinated matrices was reflected in the higher CO_2/N_2 selectivity values derived by the Ideal Adsorbed Solution Theory (IAST) for the case of 15/85 CO_2/N_2 mixture, typical of industrial fume emissions (ESI). At 273 K, the covalent frameworks exhibited a CO_2/N_2 selectivity as high as 31 and 48 for 1-FMF and 2-FMF, respectively. The selectivity of 1-FMF and 2-FMF is superior to the porous materials obtained by post-synthetic fluorination methods recently reported.[24]

Since enhanced interactions can be expected towards CH_4 owing to the polarity of C-F bond, CH_4 adsorption measurements were performed at various temperatures to characterize the process (Figure 4c and S9). The Q_{st} for F-PAF1 (17 kJ/mol) is higher compared that of the non-fluorinated analogue (14 kJ/mol)[34], which confirms the increased CH_4 affinity owing to the presence of fluorine in the porous matrix. 1-FMF and 2-FMF show a remarkably higher Q_{st} up to 20 and 24 kJ/mol, respectively. The presence of two adjacent fluorine atoms on the p-phenylene moiety increases the dipole moment and plays a key role in enhancing the interactions of the framework with CH_4. Additionally, the sub-nanometer pore size increases van der Waals stabilisation which significantly contributes to the remarkably favorable CH_4 binding energy. The Q_{st} values are compatitive with the values reported for the best performing MOFs and COFs (see Table S5 in ESI). In particular, they exceed the reported value for H-KUST-1 (18.2 Kcal/mol), a Cu(II)-based MOF whose methane adsorption properties are considered the benchmark in the field of porous materials and suitable for practical uses.[35] Futhermore, the CH_4/N_2 (50:50 mixture) and CO_2/CH_4 (50:50 mixture) selectivities were studied, using IAST theory, to evaluate the materials performance towards gas purification (ESI). 1-FMF and 2-FMF show good selectivity for both CO_2/CH_4 and CH_4/N_2 binary mixtures. In particular, the CO_2/CH_4 selectivity of 1-FMF at 273 K and 298 K of 5.4 is close that of HKUST-1 (estimated as 4.8).[36]
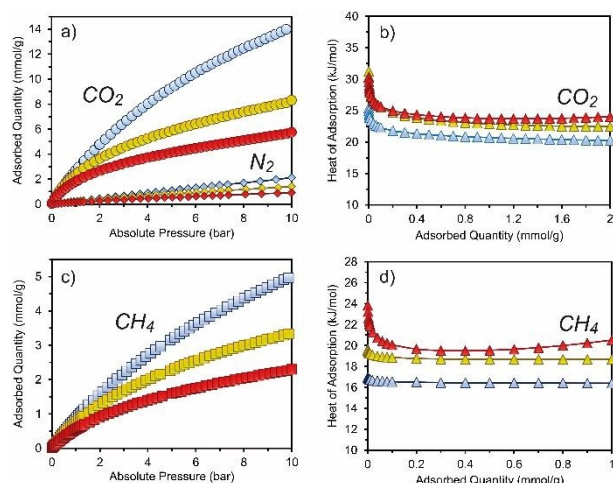
COMMUNICATION

Figure 4 CO_2 (spheres) and N_2 (diamonds) adsorption isotherms collected at 273K and up to 10 bar of F-PAF1, 1-FMF and 2-FMF (blue, yellow and red traces, respectively). b) $Q_{st}(CO_2)$ versus adsorbed quantity. c) CH_4 (squares) adsorption isotherms of F-PAF1 (blue traces), 1-FMF (yellow traces) and 2-FMF (red traces) collected up to 10 bar at a) 273 K. d) $Q_{st}(CH_4)$ versus adsorbed quantity.

In conclusion, new fluorinated organic porous materials were synthesized adopting various strategies which share the use of highly porogenic tetraphenylmethane building-units, i.e. the direct condensation of a fluorinated monomer for the formation of a new fluoro-PAF1 and by reacting two complementary functionalities of tetrahedral (A_4) and linear (B_2) struts. The synthetic protocols were successfully employed to obtain porous materials with high surface areas up to 2050 m^2/g. The CO_2 and CH_4 adsorption performances of 2-FMF show the highest Q_{st} values, owing to a higher fluorine content and microporous architecture. The results presented in this work demonstrate the active role played by fluorine-containing moieties in improving CO_2 and CH_4 capture. In particular, the calibrated introduction of fluorine groups in F-PAF1 increased the heat of adsorption for CO_2 by 53% compared to its non-fluorinated analogue.

Conflicts of interest

There are no conflicts to declare.

References

1   World Meteorological Organization, "IPCC - Intergovernmental Panel on Climate Change," http://www.ipcc.ch/, 2010.
2   G. T. Rochelle, *Science,* 2009, **325**, 1652–1654.
3   K. Sumida, D. L. Rogow, J. A. Mason, T. M. McDonald, E. D. Bloch, Z. R. Herm, T.-H. Bae and J. R. Long, *Chem. Rev.,* 2012, **112**, 724–781.
4   R. Dawson, A. I. Cooper and D. J. Adams, *Prog. Polym. Sci.,* 2012, **37**, 530–563.
5   P. Nugent, Y. Balmabkhout, S.D. Burd, A. J. Cairns, R. Luebke, K. Forrest, S. Ma, B. Space, L. Waoitas, M. Eddaoudi and M. J. Zaworotko, *Nature*, 2013, **495**, 80-84.
6   S. Kitagawa,R. Kitaura, S.-I. Noro, *Angew. Chem. Int. Ed.,* 2004, **43**, 2334-2375.
7   M. P. Tsyurupa, V. A. Davankov, *React. Funct. Polym.,* 2006, **66**, 768–779.
8   H. Furukawa and O. M. Yaghi, *J. Am. Chem. Soc.,* 2009, **131**, 8875–8883.
9   S. Das, P. Haesman, T. Ben and S. Qiu, *Chem. Rev.,* 2017, **117**, 1515–1563.
10 N. B McKeown, P. M. Budd, K. J. Msayib, B. S. Ghanem, H. J. Kingston, C. E. Tattershall, S. Makhseed, K. J. Reynolds and D. Fritsch, *Chem. Eur. J.*, 2005, **9**, 2610-2620.
11. T. Ben, H. Ren, S. Ma, D. Cao, J. Lan, X. Jing, W. Wang, J. Xu, F. Deng, J. M. Simmons, S. Qiu and G. Zhu, *Angew. Chem. Int. Ed.*, **2009**, *48*, 9457-9460.
12 Y. C. Zhao, D. Zhou, Q. Chen, X. J. Zhang, N. Bian, A. Di Qi and B. H. Han, *Macromolecules* 2011, **44,** 6382–6388.
13 S. Bracco, D. Piga, I. Bassanetti, J. Perego, A. Comotti and P. Sozzani, *J. Mater. Chem., A* 2017, **5**, 10328–10337.
14 Z. Z. Yang, Y. Zhao, G. Ji, H. Zhang, B. Yu, X. Gao and Z. Liu, *Green Chem.* 2014, **16**, 3724–3728.
15 Z.-Z. Yang, Y. Zhao, H. Zhang, B. Yu, Z. Ma, G. Ji and Z. Liu, *Chem. Commun.* 2014, **50**, 13910–13913.
16 J. Perego, D. Piga, S. Bracco, P. Sozzani and A. Comotti, *Chem. Commun.* 2018, **54**, 9321–9324.
17 X. Yang, L. Zou and H. C. Zhou, *Polymer,* 2017, **126**, 303–307.
18 L. Zou, Y. Sun, S. Che, X. Yang, X. Wang, M. Bosch, Q. Wang, H. Li, M. Smith, S. Yuan, Z. Perry and H.-C. Zhou, *Adv. Mater.,* 2017, **29**, 1700229.
19 Y. Zhang, B. Li and S. Ma, *Chem. Commun.,* 2014, **50**, 8507–8510.
20 C. Klumpen, M. Breunig, T. Homburg, N. Stock and J. Senker, *Chem. Mater.,* 2016, **28**, 5461–5470.
21 S. J. Garibay, M. H. Weston, J. E. Mondloch, Y. J. Colón, O. K. Farha, J. T. Hupp and S. T. Nguyen, *CrystEngComm,* 2013, **15**, 1515–1519.
22 G. Xing, I. Bassanetti, S. Bracco, M. Negroni, C. Bezuidenhout, T. Ben, P. Sozzani and A. Comotti, *Chem. Sci.,* 2019, **10**, 730-736.
23 Y. Zhao, K. X. Yao, B. Teng, T. Zhang and Y. Han, *Energy Environ. Sci.,* 2013, **6**, 3684–3692.
24 A. Alahmed, M. E. Briggs, A. Cooper and D. Adams, *J. Mater. Chem. A,* 2019, **7**, 549-557.
25 D. P. Liu, Q. Chen, Y. C. Zhao, L. M. Zhang, A. Di Qi and B. H. Han, *ACS Macro Lett.,* 2013, **2**, 522–526.
26 A. Comotti, S. Bracco, T. Ben, S. Qiu and P. Sozzani, *Angew. Chem. Int. Ed.*, 2014, **53**, 1043-1047.
27 A. Comotti, S. Bracco and P. Sozzani, *Acc. Chem. Res.*, 2016, **49**, 1701−1710.
28 P. Lama, H. Aggarwal, C. X. Bezuidenhout and L. J. Barbour, *Angew. Chem. Int. Ed.*, 2016, **55**, 13271-13275.
29. A. Comotti, S. Bracco, L. Ferretti, M. Mauri, R. Simonutti and P. Sozzani, *Chem. Comm.* **2007**, 350-352.
30. P. Sozzani, S. Bracco, A. Comotti, M. Mauri, R. Simonutti and P. Valsesia, *Chem. Comm.* **2006**, 1921-1923.
31 Y. Li, T. Ben, B. Zhang, Y. Fu and S. Qiu, *Sci. Rep.*, 2013, **3**, 2420.
32 R. E. Dorris, W. C. Trendell, R. A. Peebles and S. A. Peebles, *J. Phys. Chem. A,* 2016, **120**, 7865−7872.
33 A. Comotti, S. Bracco, A. Yamamoto, M. Beretta, T. Hirukawa, N. Tohnai, M. Miyata, and P. Sozzani, *J. Am. Chem. Soc.*, 2014, **136,** 618−621.
34 T. Ben, C. Pei, D. Zhang, J. Xu, F. Deng, X. Jing and S. Qiu, *Energ. Environ. Sci.*, 2011, **4**, 3991–3999.
35 K. Konstas, T. Osl, Y. Yang, M. Batten, N. Burke, A. J. Hill and M. R. Hill, *J. Mater. Chem.,* 2012, **22**, 16698–16708.
36 L. Hamon, E. Jolimaître and G. D. Pirngruber, *Ind. Eng. Chem. Res.,* 2010, **49**, 7497–7503.
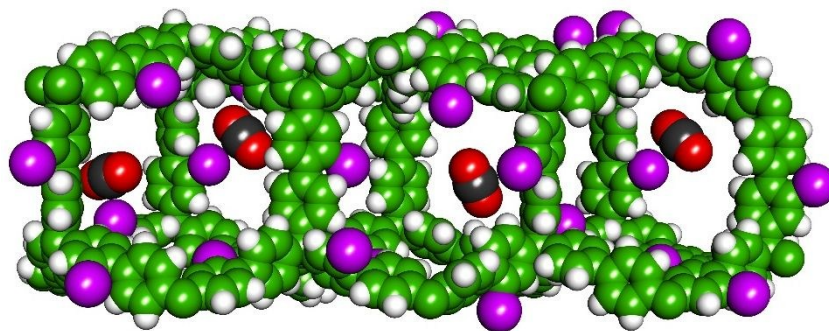
COMMUNICATION

Journal Name

Table of Contents

Hyperpolarized ^{129}Xe NMR highlights open porosity of fluorinated organic frameworks which show CO_2 and CH_4 capture with high selectivity towards N_2.